Amplitudes of regional seismic phases in relation to crustal structure of the Sierra Nevada, California

A. Paul,[1] D. Jongmans,[2] M. Campillo,[1] P. Malin,[3] and D. Baumont[1]

Abstract. We have recorded and modeled the amplitudes of regional seismic waves produced by the Nevada Test Site Non Proliferation Experiment explosion along a 400-km profile across the southern Sierra Nevada of California. Along this profile the amplitudes of the crustal phases Pg and Lg decrease monotonically with distance because of the cumulative effects of geometrical spreading and a frequency-dependent crustal attenuation given by $Q \simeq 138 f^{0.76}$ ($1 \leq f \leq 8$ Hz). This observation implies that the crust of the Sierras is not more attenuative to P and S waves than the crusts of the adjacent Great Valley and Basin and Range. The only amplitude anomaly related to the crustal structure is a strong attenuation of Lg on the vertical component in the Great Valley due to the refraction of rays in the low-velocity sediments of the basin. In contrast to Pg and Lg, Pn amplitude increases across the Sierra Nevada and the eastern edge of the Great Valley. Then, some 30 km west of the exposed Sierran batholith, the amplitude of Pn suddenly decreases by a factor of 10. On the basis of a new refraction model produced by the Southern Sierra Nevada Continental Dynamics study and on numerical simulations of the Pn/Pg energy ratio, these changes in Pn amplitude are shown to be due to a local increase in crustal thickness, from roughly 35 to 45 km, centered under the western Sierra. The size and location of the amplitude anomaly can be explained with a gently sloping two-layer crust-mantle model with P velocities of 6.0 km/s and 8.0 km/s. The small offset crustal root focuses Pn waves toward the westernmost Sierra Nevada and the easternmost Great Valley, significantly increasing the Pn energy in these regions. The focusing effects diminish rapidly toward the west as the Moho is again horizontal.

Introduction

The study of path effects on the amplitudes of short-period regional seismic phases has long been a subject of interest to seismologists. The Lg, Pg, and Pn phases are used in discriminants between nuclear tests and other seismic sources [e.g., *Walter et al*, 1995]. Because the regional wave field consists of waves multiply reflected in the crustal waveguide (Pg and Lg) and refracted at the crust-mantle boundary (Pn), it is very sensitive to lateral heterogeneity of the crust. To improve the effectiveness of regional discriminants and to investigate the potential of regional phases in the exploration of crustal

structures in regions where they are still poorly known, there is a need for a better understanding of path effects on regional phases.

Among the most spectacular examples of path effects is the strong decay or extinction of the Lg phase that has been reported for travel paths crossing mountain ranges and high plateaus such as the Tibetan Plateau [*Ruzaikin et al.*, 1977; *Ni and Barazangi*, 1983], the Urals [*Baumgardt*, 1990], the Andes [*Chinn et al.*, 1980], the Alps [*Campillo et al.*, 1993], and the Pyrénées [*Chazalon et al.*, 1993]. In the cases of the Alps and Pyrénées, numerical simulations show that the extinction of Lg cannot be explained by the lateral variations in Moho depth or even lithospheric overthrusting. Instead the amplitude anomalies are due to small-scale heterogeneity within the crust which induces strong attenuation of the Lg wave [*Campillo et al.*, 1993]. To understand how regional seismic waves are affected by a particular type of crustal heterogeneity, a detailed seismological study is required, including careful measurement of the geometry and velocity structure of the crustal waveguide and numerical simulations of wave propagation. In this paper we report on such a study performed in the southern part of the Sierra Nevada in California and conducted by the Southern Sierra Nevada Continental Dynamics

[1]Laboratoire de Géophysique Interne et Tectonophysique, Centre National de la Recherche Scientifique, and Université Joseph Fourier, Grenoble, France.

[2]Laboratoire de Géologie de l'Ingénieur et d'Hydrogéologie, Université de Liège, Belgium.

[3]Department of Geology, Duke University, Durham, North Carolina.
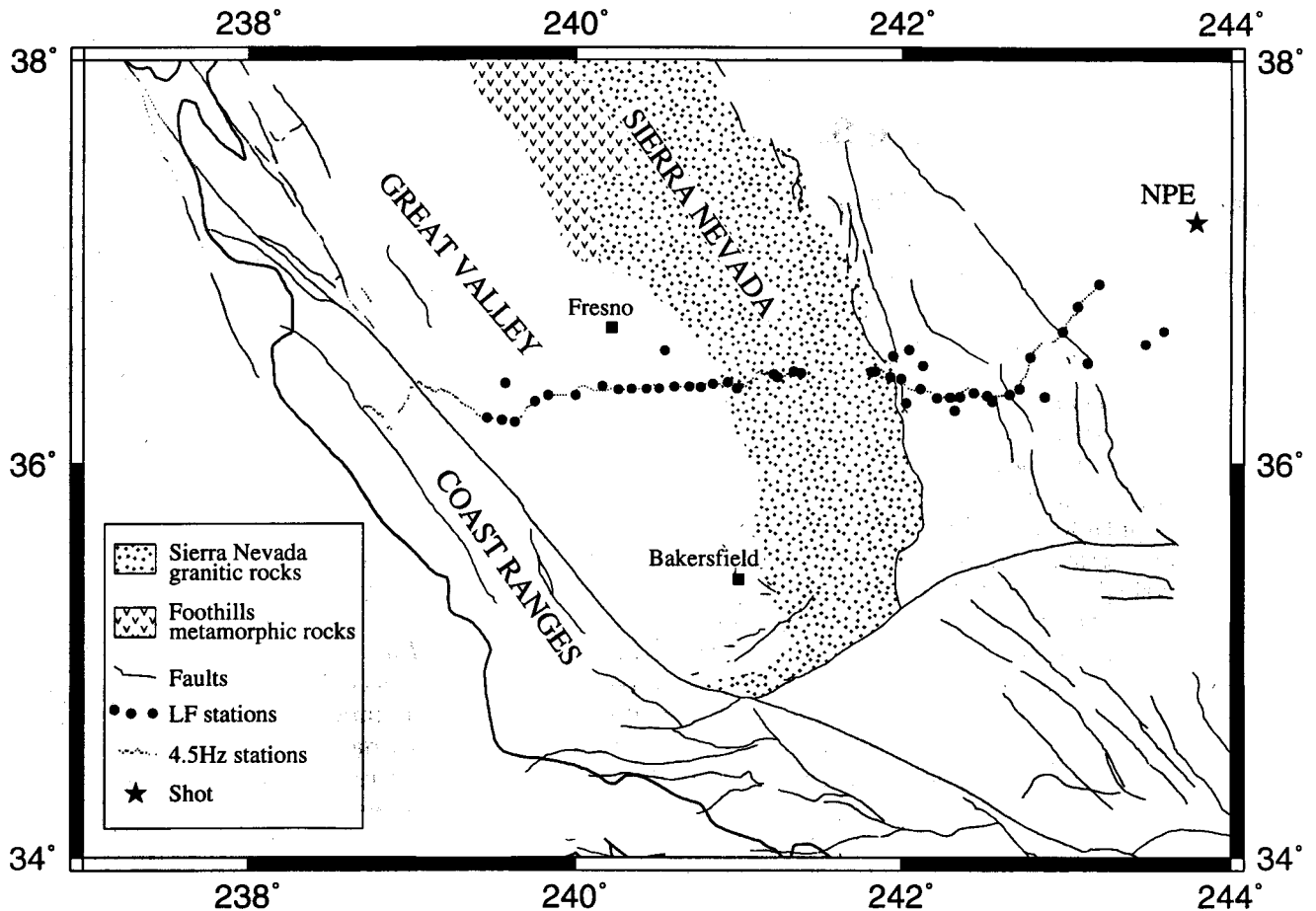
Figure 1. Location map of the experiment. Solid circles represent low-frequency (1 Hz or below) two- or three-component seismic stations. Dotted line shows stations with 4.5 Hz vertical sensors set up to record refraction data from the NPE explosion at the Nevada Test Site.

(SSCD) project in September 1993 [*Wernicke et al.*, 1996; *Fliedner et al.*, 1996].

In conjunction with the refraction profiles, magnetotelluric profiles, and teleseismic observations of converted waves carried out by the SSCD group, we collected a set of regional seismic wave data, using a variety of portable seismographs. The data set that we discuss here is a 400 km east-west profile from the 1 kt Non Proliferation Experiment (NPE) explosion detonated at the Nevada Test Site [*Keller et al.*, 1994]. The profile starts 65 km southwest of the Nevada Test Site and ends at the Coast Ranges, 25 km west of Coalinga (Figure 1). Along this profile we deployed 14 three-component stations with 1-s sensors and seven three-component stations with 20-s sensors at roughly equal spacings. Along the east and west sides of the Sierras the gaps between these stations were covered with 30 two-component (vertical and radial) stations with 1-s geophones. In the high Sierras the gap was shortened by two short-period three-component stations from two SSCD high-country teleseismic observation arrays [*Phinney et al.*, 1994]. This data set is referred to hereafter as the "low-frequency" dataset.

In addition to our instruments, the NPE explosion was also recorded along this same profile by 269 stations with vertical 4.5-Hz sensors spaced at nearly equal intervals of about 1 km [*Keller et al.*, 1994]. We refer to this as the "refraction" data set. The combined data sets allow us to investigate the evolution of regional phases as they propagate along the profile with a very good spatial resolution and in several frequency ranges.

Our focus here is to document and model the amplitude variations of the seismic phases Pn, Pg, and Lg across the southern Sierras and in the surrounding Owens Valley and Great Valley. Variations in amplitude are considered anomalous if they cannot be explained by the geometrical spreading or by a frequency-dependent attenuation related to an average value of the Q factor for the crust. Because amplitude anomalies are present, we will investigate the velocity structure and the crustal geometry that produce them. Of particular interest is the propagation of Lg waves through the Sierras because this phase is known to be affected by some of the changes in crustal structure associated with mountain ranges [e.g., *Campillo et al.*, 1993].

Since our data set was collected with different types

of recorders and sensors, special processing is required to calibrate the amplitudes for meaningful station-to-station comparisons. Once this calibration is achieved, we use the decay rate of Lg and Pg energy along the profile to measure the average crustal Q factors for P and S waves to infer their frequency dependence. The spatial amplitude variations of Lg and Pg waves are then investigated for differences in the attenuation of P and S waves as they propagate in the crustal waveguide. Finally, we find that the Pn phase exhibits an anomalous increase of amplitude at stations within the eastern part of the Great Valley. We numerically model this increase, using the simple crustal model deduced from the SSCD refraction studies.

Data Preprocessing

The low-frequency data set was recorded by using two different types of instruments (Refteks and U.S. Geological Survey analog 5-day recorders) and four different types of sensors. The sensors included three-component CMG-40s with natural periods of 20 s, three-component L4Cs with natural periods of 1 s, and one-component L4s and EV-17s, both with natural periods of 1 s. In order to establish the amplitude calibrations of each type of station (receiver plus sensor), a few sites were equipped with multiple instruments and/or sensors. Thus we were able to cross-check the calibration factors of the analog recorders and the impulse response of the sensors.

The first step in the processing is to convert all the amplitudes to volts. Then the resulting seismograms are deconvolved from their sensor response and reconvolved by the theoretical response of the L4 (natural frequency, 1 Hz; damping factor, 0.7) to eliminate the amplitude differences introduced by the use of different sensors. This procedure removes most of the low-frequency content of the few broadband stations. However, previous checks indicate that the signal-to-noise ratio is poor above 3-s period at stations located more than 170 km from the source. Finally, the seismograms are filtered in the frequency band 1-4 Hz. This passband is chosen to give the best waveform comparisons among data acquired with different sensors.

After careful trace editing, the final low-frequency data set includes 43 vertical, 41 radial, and 21 transverse seismograms with offsets ranging from 65 to 400 km. The preprocessing cannot suppress all amplitude variations related to the heterogeneity of the recording network. To eliminate them, each seismogram is normalized by the energy measured in a given time window of the same seismogram (e.g., the Pg time window) before starting amplitude computations.

All seismograms from the refraction data set were recorded with the same one-component 4.5-Hz sensor and two different types of recording instruments. Indeed, the change in instrument coincides with a strong change in the amplitude of the seismograms. How-

ever, without knowing the instrumental response we preferred not to apply any correction.

Amplitude Analysis of Pg and Lg

The amplitudes of the crustal phases Pg and Lg vary with distance from the source because of a combination of factors:

1. Local site effects include all phenomena that produce amplitude variations between one receiver and its neighbors (e.g., the quality of the coupling of the sensor to the soil and local amplification). Our purpose is to study amplitude variations on a regional scale (>50 km). Since the distance between receivers is, on average, 15 km for the low-frequency data set and 1 km for the refraction data set, spatial sampling is sufficient to avoid misinterpreting local site effects as regional amplitude anomalies. Moreover, most of this study relies on amplitude variations measured after normalization of each seismogram by its energy in a given time window (centered on the Pg or Lg arrival). This is a crude but efficient method to attenuate amplitude variations at short spatial wavelengths, including some of the site effects and the remnants of instrumental corrections. The technique of normalization and its influence on our observations will be discussed in greater detail later.

2. The geometrical spreading factor is well known in both space and time for the Lg phase [e.g., Nuttli, 1973]. At regional distances (>150 km) the Lg phase is the superposition of S waves multiply reflected in the crustal waveguide. Thus it is totally trapped in the crust, and its spectral energy density decreases slowly with distance. Campillo et al. [1984] have used synthetic seismograms to evaluate the decay rate of Lg in the time domain (i.e., the geometrical spreading needed to correct the spectral density per time unit). They found that this decay rate is $d^{-0.83}$ (d, epicentral distance). In the simulations they used a 30-km-thick continental crust with a one-dimensional velocity structure similar to the average velocity model for our region. Thus we have used their result. The geometrical spreading of $d^{-0.83}$ was also measured from real data and proposed by Nuttli [1973] from the higher-mode surface wave representation of Lg.

Within the range of epicentral distances considered here (150-400 km) the Pg wave train also is formed mainly by P waves multiply reflected between the Moho and the surface. Numerical simulations show that the direct and refracted waves have weak amplitudes and a negligible contribution to the Pg wave train at regional distances. However, the trapping of the Pg wave in the crust is much less efficient than that of Lg, since part of its energy is continuously converted into mantle S waves at the Moho. The numerical study by Campillo et al. [1984] indicates that its geometrical spreading is approximately $d^{-1.50}$.

3. In the case of weak attenuation, frequency-dependent attenuation of wave spectral energy density is

due to anelastic attenuation and scattering and can be expressed using a frequency-dependent quality factor.

4. As was noted earlier, amplitude variations due to crustal structure are well known for the Lg phase. Because its trapping is less efficient, the variations of Pg amplitude with distance make precise evaluation of structural effects on its propagation more difficult. Since our profile crosses a mountain range with varying Moho depth and a large sedimentary basin, for which the internal structures are known from refraction data, this is a good experiment to study propagation anomalies if they exist.

Estimation of the Average Q Factor for P and S Waves

To evaluate the S and P wave mean crustal quality factor, we measure the decay rate of Lg and Pg spectral energy density with distance. In the time window providing the largest amplitudes (i.e., the time window centered on the group velocity 3.2 km/s for Lg and 5.4 km/s for Pg) we calculate the natural logarithm of the spectral amplitude per unit time as a function of epicentral distance. For each station i and frequency f this amplitude can be written as

$$|A_i(f)|/\Delta t = A_0(f)d^{-gs}e^{-\pi f d/Qv}$$

where Δt is the width of the time window, $gs = 0.83$ for Lg and 1.50 for Pg, d is the epicentral distance, Q

is the quality factor, and v is the group velocity. Thus the logarithm of $|A_i(f)|d^{gs}/\Delta t$ is a linear function of distance d with a slope proportional to $1/Q$. At each frequency f, a linear regression of $\log(|A_i(f)|d^{gs}/\Delta t)$ with respect to d gives an estimate of the average crustal Q factor.

Using 95 records of the low-frequency data set (38 vertical , 37 radial, and 20 transverse components), we make these computations for the group velocity of 3.2 km/s (Lg phase) for 32 values of frequency between 1 and 4 Hz. By modeling the frequency dependence of Q by $Q_0 f^n$, we find $Q_{Slf} = 140 f^{0.94}$, where the subscript lf refers to the name of the data set (low-frequency) used for the estimate. The estimated values of Q_{Slf} and the linear correlation coefficient are plotted as a function of frequency in Figure 2a (top panel). The bottom panel in Figure 2a shows an example of the linear regression on spectral amplitude with respect to distance at 1.36 Hz (close to the dominant frequency). This panel shows that the amplitude values are scattered around the regression line. This distribution explains the low values of the linear correlation coefficient shown in the top panel. The quality of the linear regression is even lower when we try to estimate Q_{Plf} at the group velocity of 5.4 km/s from the same data set. Therefore no results of this calculation are presented here.

In an attempt to improve the measurement of the Q factor, similar estimates are also made from the traces of the refraction dataset recorded with the same instru-
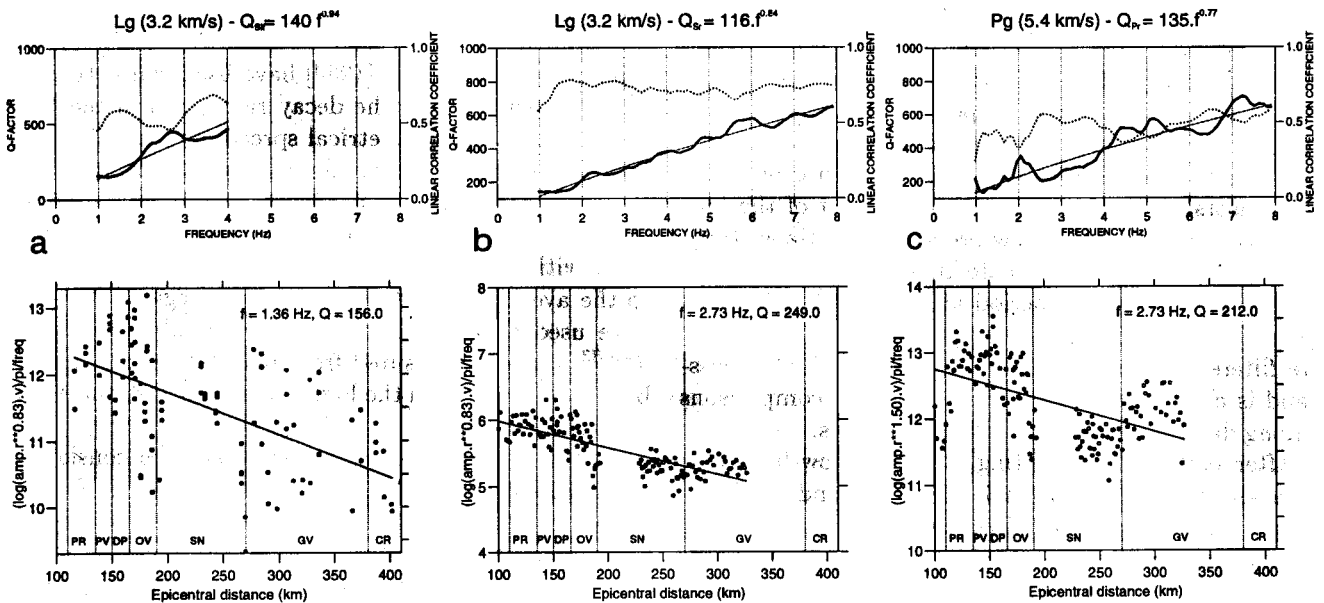
Figure 2. Estimates of the Q factor using a linear regression on the spectral amplitude with respect to distance. Top panels show estimated values of Q (thick solid line) as a function of frequency, best fitting $Q_0 f^n$ curve (thin solid line), and values of the linear correlation coefficient (dotted line). Bottom panels show examples of linear regressions used to evaluate Q. The vertical dotted lines separate the different geological provinces crossed by the profile (PR, Panamint Range; PV, Panamint Valley; DP, Darwin Plateau; OV, Owens Valley; SN, Sierra Nevada; GV, Great Valley; CR, Coast Ranges). (a) Estimate of Q_S at the Lg dominant group velocity (3.2 km/s) from all the available components of the low-frequency data set. (b) Estimate of Q_S from the refraction data set (vertical component only). (c) Estimate of Q_P from the refraction data set at the dominant group velocity of the Pg phase (5.4 km/s).

ments. Figure 2b shows the results obtained for the Lg wave train (Q_{Sr}), and Figure 2c shows those obtained for the Pg wave train (Q_{Pr}) (the subscript r indicates refraction). As revealed by the higher values of the linear regression coefficient the refraction data set gives a better estimate of Q_S. We believe that the higher quality of these last measurements is due to the larger number of seismograms available for the analysis (143) and, above all, to the homogeneity of the recording instruments. Within the frequency band 1-8 Hz we obtain $Q_{Sr} = 116f^{0.84}$ and $Q_{Pr} = 135f^{0.77}$. The expression for Q_{Sr} is similar to the one inferred for Q_{Slf}. Moreover, Q_{Pr} and Q_{Sr} (or Q_{Slf}) are close to one another, showing that the mean crustal quality factors for P and S waves and their dependence on frequency are comparable between 1 and 8 Hz along this profile.

Noting that Q_{Pr}, Q_{Sr}, and Q_{Slf} have similar variations with frequency, we can estimate the average $Q(f)$ using all 176 measurements of $Q_{Pr}(f)$, $Q_{Sr}(f)$, and $Q_{Slf}(f)$ with the same weighting in a fit to a single $Q_0 f^n$ model. We find an estimated crustal Q value of $138f^{0.76}$, $1 \le f \le 8$ Hz $(Q_P \simeq Q_S)$, similar to previous estimates of Q_S made in the western United States by *Singh and Herrmann* [1983], *Nuttli* [1986], or *Chavez and Priestley* [1986].

The bottom panels of Figure 2 show that the sign of the difference between the observed spectral amplitudes and the predicted values changes across the boundaries of the tectonic provinces (indicated along the x axis by vertical dotted lines). This progression is clear in Figures 2b and 2c, in which all measured amplitudes are weak in the Sierra and strong on either side when compared to the regression line. In Figure 2a, amplitudes display considerable scatter in the valleys (Owens Valley and Great Valley), which may be due to strong site effects. These observations are the first indications of large-wavelength amplitude variations correlated with regional geology.

Normalization by Pg Energy

Since we are interested in large-scale amplitude effects, we normalize the seismograms with respect to Pg in order to remove the short-wavelength amplitude variations. Pg is the most logical choice for this normalization, since it is the most energetic of the three phases Pn, Pg, and Lg at all stations and therefore the most stable phase in our records. Because of the large range of shallow velocity structures encountered along the profile, wave fields recorded at the surface have different polarizations in different regions. Since normalizing each component separately would modify the amplitude ratios between the components, we normalize amplitudes of all components by the maximum energy of the Pg phase in the propagation plane. This procedure is carried out in three steps. First, we compute the total amplitude in the propagation plane from the amplitudes on the vertical and radial components $(a(t) = [v^2(t) + r^2(t)]^{1/2})$. Then we compute the to-
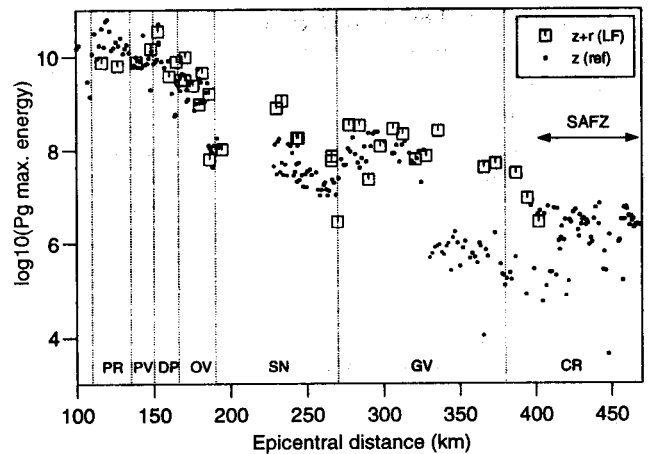
Figure 3. Common logarithm of Pg maximum energy measured in the group velocity window (5.2-5.7 km/s) as a function of offset (see text for explanations of the computation method). The open squares are measured from the vertical and radial components of the low-frequency seismograms, and the solid circles are measured from the refraction data set using only vertical components. The location of the San Andreas Fault Zone (SAFZ) is shown.

tal energy of $a(t)$ within a sliding Gaussian window (of half width increasing linearly with epicentral distance to account for spreading in time). Finally, we take the maximum value of the energy in the group velocity window 5.7-5.2 km/s (Pg phase) as the normalization factor of each seismogram.

The common logarithms of these normalization factors are plotted as open squares as a function of offset in Figure 3. The Pg maximum energy computed from the vertical seismograms of the refraction data set is also shown (as solid circles) on the figure. In the Sierra Nevada, energies measured by adding vertical and radial components (squares) are clearly larger than those measured only on vertical components (circles), while they are similar in other parts of the profile at distances shorter than 330 km. This difference results from a difference in the polarization angle. Within the Sierra Nevada there is no low-velocity sedimentary cover, and Pg is incident on the surface at a nonvertical incidence. Energy is therefore recorded on both radial and vertical components. In Owens Valley and Great Valley the tabular and thick sedimentary covers decrease the incidence angle of the rays and concentrate Pg energy on the vertical component.

At 330 km distance, energies measured from the refraction data set undergo a sharp decrease. Since this location corresponds precisely to the change in instrument type, it can be attributed to the lack of instrument response correction in this data set. No similar explanation can be found for the sudden increase in amplitude occurring at 420 km upon entering the San Andreas Fault Zone. Moreover, a similar increase in wave amplitudes has already been observed by *Wald*

and Heaton [1991] on *Lg* and *Rg* phases recorded by the permanent stations of the California networks. With a more densely spaced data set we also note the sharpness of the amplitude increase. This sharpness suggests that the amplitude increase is due to a lateral change in rock type rather than a lateral decrease in Moho depth.

Wald and Heaton [1991] also described an amplification of *Lg* and *Rg* in the Great Valley, although the number of permanent stations in the Great Valley is small and their study relied only on vertical component seismograms. However, Figure 3 confirms that this amplification exists for the *Pg* wave train. It cannot be attributed to a change in polarization angle, since our data are three-component seismograms. This large-scale amplification of *Pg* is probably related to the sedimentary basin. Similar amplifications probably exist in Owens Valley, as indicated by the strong change in *Pg* energy measured between the hard rock sites of the Sierran foothills and the other sites located in the middle and eastern part of the valley (Figure 3).

According to Figure 3, normalizing seismograms by *Pg* maximum energy has three effects. First, it removes the short-wavelength variations which scatter the ob-served amplitude values. Second, it corrects the amplitudes of all the wave trains for the geometrical spreading and attenuation related to the *Q* factor of the *Pg* phase. Third, it corrects amplitudes for the large-wavelength amplification of *Pg* in the Great Valley. However, the normalization can lead to an overcorrection of phases not affected by the amplification.

Lg/Pg Energy Ratio

Seismograms normalized with respect to *Pg* maximum energy are presented in the top panels of Figures 4a (vertical component) and 4b (radial component). The time axis t is replaced by a group velocity axis $v = d/t$ (where d is the epicentral distance) so that the phases *Pn*, *Pg*, and *Lg* line up on the plot irrespective of offset. From the normalized seismograms we build the energy diagrams presented in the bottom panels of Figures 4a and 4b. The processing used to obtain these maps is close to the one described previously to measure the *Pg* maximum energy. For each seismogram an energy trace is computed by summing the squares of the amplitudes in a sliding Gaussian time window
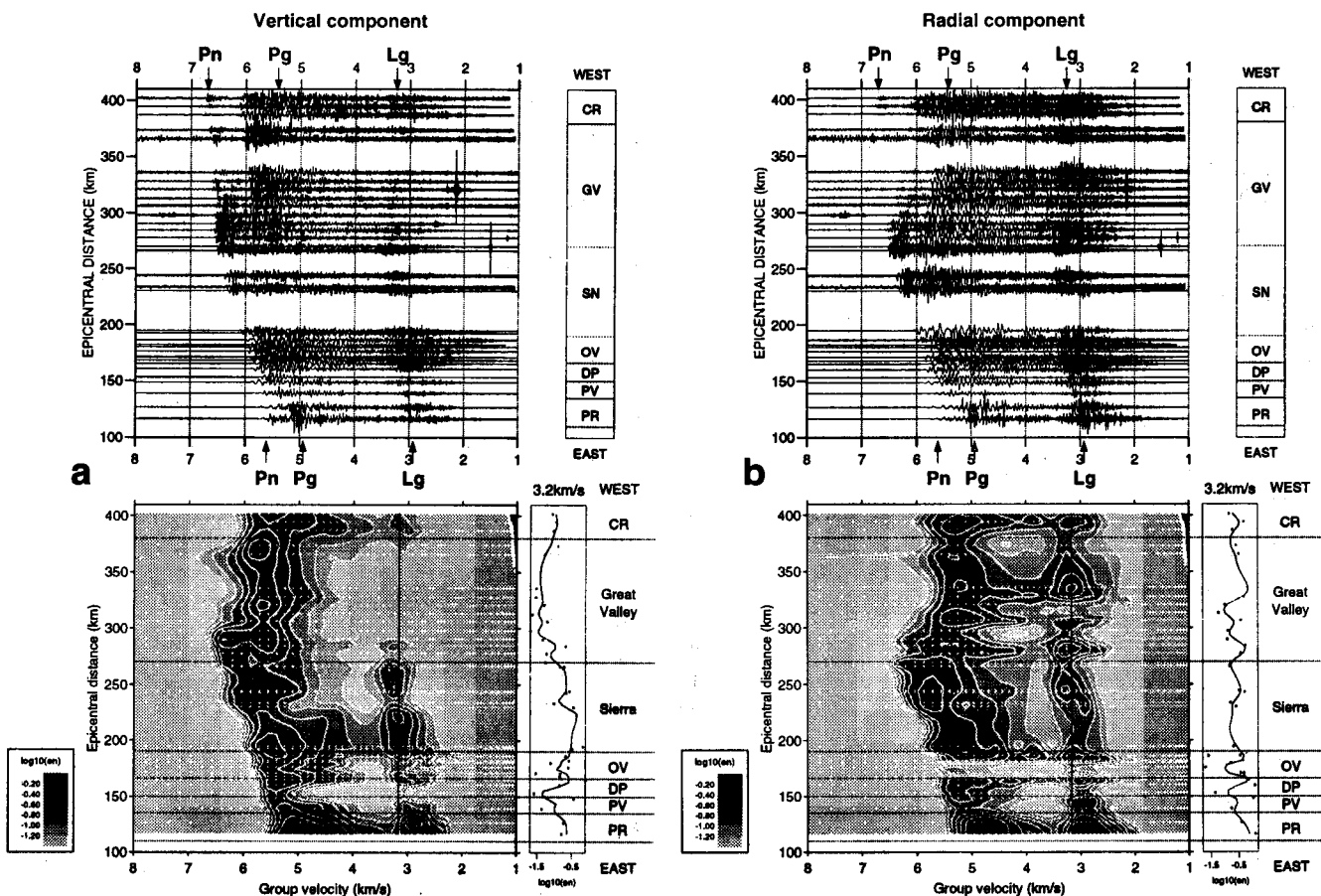
Figure 4. Seismograms and energy maps after normalization by the maximum energy of the Pg phase presented in Figure 3. (a) Vertical component; (b) radial component. The contour maps plotted in the bottom panels show variations of the common logarithm of energy as a function of group velocity and epicentral distance. The white dots indicate locations where measurements are made. A cross section of the energy map at the main Lg group velocity (3.2 km/s) is plotted on the right-hand side. Energy of Lg as measured from the normalized seismograms is shown by dots. The result of the 2-D bilinear interpolation is shown by the solid line.

centered on different values of the group velocity. To account for the dispersion of wave trains with increasing offset, the time window half width is taken equal to $\Delta t_0(s) = d(km)/200$, where d is the offset. The final energy maps shown in Figures 4a and 4b are obtained by two-dimensional bilinear interpolation of the energy traces. This processing enhances the major trends of energy variations with epicentral distance and group velocity at the expense of short-wavelength variations.

The energy maps of Figure 4 show that Lg propagates across the whole profile. This pattern is particularly clear on the radial component around the group velocity 3.2 km/s. To illustrate the variations of the Lg/Pg energy ratio, cross sections at 3.2 km/s are plotted on the right-hand side of the maps. These plots indicate the quality of the 2-D bilinear interpolation, which provides continuous curves fitting correctly the measured points plotted as dots. When only large-scale variations are considered, cross sections show that the vertical component of Lg undergoes much stronger variations with offset than the radial component, which remains almost constant around -0.5. Moreover, these variations of the vertical component are correlated with geological boundaries. Lg energy on the vertical component is stronger in the Sierra and weaker on either side, with a marked negative anomaly in the Great Valley.

To study these correlations in detail, we plot the Lg/Pg energy ratios for all the components at the same scale in Figure 5. The thick plain line corresponds to the theoretical variation with distance of the Lg to Pg energy ratio at 1 Hz. Since the spectra of Pg and Lg are not restricted to this single frequency, the ratio computed at 1 Hz is only an approximation of the ratio of total energies. The approximation can be used because

1 Hz is the dominant frequency. The theoretical energy ratio is computed using the expressions of amplitude decay due to geometrical spreading and Q factor measured previously:

$$\log_{10}(ER(d)) = E_0 + 2(1.50 - 0.83)\log_{10}(d)$$
$$+2\pi d\log_{10}(e)(1/v_P - 1/v_S)/Q_1$$

where d is the epicentral distance, e is the basis of natural logarithms, v_P and v_S are the group velocities of Pg and Lg, and Q_1 is the mean value of the quality factors for both P and S waves at 1 Hz ($Q_1 = 140$). Figure 5 shows that the observed Lg/Pg energy ratio on the horizontal components (r and t) varies with epicentral distance as predicted by the theory. On the contrary, there is a discrepancy between the vertical component and the theoretical curve in the Great Valley, where the Lg/Pg energy ratio is nearly 10 times less energetic than what is predicted by the theory. This difference results from the change in incidence angle associated with the thick, tabular, and low-velocity sedimentary sequence of the Great Valley. At the surface of the valley the S waves which make up the Lg phase are mostly polarized on the horizontal components, because the rays are incident nearly vertically. The same result is also valid for the refraction data set.

In order to study the correlation between the total Lg energy and the geological provinces we must eliminate the polarization effects described above. This step is done by adding the amplitudes of the radial and vertical components as in the processing applied to Pg. We find that the total energy of Lg, as Pg, is amplified in the Great Valley. The low values of the Lg/Pg energy ratio measured from the vertical component of Lg and plotted in Figure 5 result from the normalization by the Pg energy. In the Great Valley there is no Lg on the vertical component. Since noise amplitude does not vary with the distance, the normalization by the strong values of Pg total energy in the Great Valley (see Figure 3) leads to low values of the Lg/Pg ratio on the vertical component.

Results of the amplitude analysis of Pg and Lg phases can be summarized as follows. The study of Lg and Pg amplitude decay with distance leads to crustal Q_S and Q_P values close to previous estimates of Q_S made in the western United States. The total energies of both Pg and Lg, computed by adding the vertical and radial components, show a regular decrease with distance from the source. The only remarkable amplitude anomaly is an amplification of Pg and Lg in the Great Valley. The amplitudes of the horizontal components of Lg decrease with respect to Pg as predicted by theoretical expressions for geometrical spreading and attenuation. Thus neither phase is affected by variations in the crustal structure. The thick sedimentary sequence of the Great Valley modifies the incidence angle of the rays, making the Lg phase almost disappear on the vertical components (and similarly for the Pg phase on the horizontal
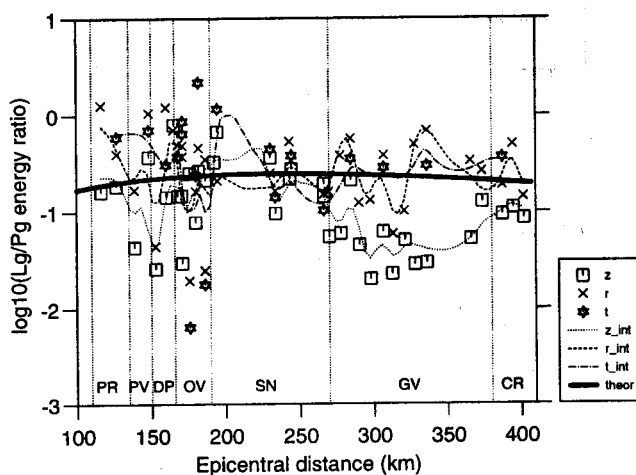
Figure 5. Lg/Pg energy ratio measured on the different components of the seismograms (z, vertical; r, radial; t, transverse). Results of the bilinear interpolation used to build the energy maps corresponding to each component are shown by dotted lines. The theoretical ratio computed by considering the amplitude decays of Pg and Lg with distance due to geometrical spreading and Q factor is shown by the thick solid line.

components). Both data sets show that the *Pg* and *Lg* crustal phases suffer no extinction or attenuation in propagation through the Sierra Nevada.

Amplitude Analysis of the *Pn* Phase

Pn is the fastest wave train present in our data set. Figure 4 shows that it separates from *Pg* around 200 km and its group velocity increases from 6 to 6.8 km/s. The other mantle head wave, *Sn*, is not visible because it is hidden by the strong *Pg* coda. *Pn* amplitudes on the vertical component are similar to those of *Pg* to a distance of 300 km where they decrease abruptly (Figure 4a). *Pn* amplitudes on the radial component decrease more gradually from 270 km (Figure 4b). To characterize the *Pn* amplitude anomaly, we measured the variations with offset of its total energy and the variations of the polarization angle of the particle motion associated with the *Pn* phase (Figure 6). Since the group velocity of the *Pn* phase is not constant in the offset range (150-400 km), which is close to the critical distance, we cannot proceed as with the *Lg* phase.

Instead, the analysis is as follows. First, arrival times are picked from the raw seismograms (i.e., without any station correction), and a 3-s time window is extracted from each record starting at the chosen arrival time. Second, the polarization angle of the particle motion associated with the *Pn* arrival is measured in the radial-vertical plane within the 3-s time window by using a 2-D covariance matrix analysis [e.g., *Kanasewich*, 1975]. Results of this two-step analysis are presented as a function of epicentral distance in the top panel of Figure 6. The particle motion associated with the *Pn* phase is nearly vertical (at 80° to 90° from the horizontal) in the Darwin Plateau (DP), Owens Valley (OV), and the Great Valley (GV), whereas it is polarized at 40° from the horizontal in the Sierra Nevada (SN). The change in polarization occurs close to the edges (within 10 km) of the exposed Sierran batholith. It is due to the shallow low-velocity sediments of the valleys, which increase the incidence angle of the rays with respect to the horizontal, as explained earlier for *Lg*. The change in polarization angle explains that, on the radial component, the largest amplitudes of the *Pn* phase are observed within the Sierra Nevada (nonvertical incidence) and start decreasing when entering the Great Valley at 270 km (close to the vertical incidence), as shown in Figure 4b. Similarly, the change in polarization should weaken amplitudes of the vertical component in the Sierra Nevada and strengthen them elsewhere. However, the amplitude decrease of the vertical component is observed not at the western margin of the Sierra batholith (270 km), but rather in the Great Valley, at 300 km, where there is no change in the polarization angle. The best explanation is a structure-related amplitude anomaly, which changes the amplitude of *Pn* but not that of *Pg* or *Lg*.

To evaluate the *Pn* amplitude changes with more accuracy, we compute the total energy in the 3-s time window of the seismograms normalized with respect to *Pg*. We add the vertical and radial components. Its variations with offset are plotted as open squares in Figure 6 (bottom panel). The dots show the total energy values computed from the refraction data set (vertical components only). Both data sets show a progressive increase in *Pn* energy (with respect to *Pg*) from 150 km to 290-300 km, where a rapid and strong decrease is observed. From 310 km to the end of the profile the *Pn*/*Pg* energy ratio remains constant. Within 15 to 20 km and 30 km beyond the western boundary of the Sierra batholith the *Pn* total energy is reduced by a factor of 10 with respect to the *Pg* maximum energy. This reduction is not an effect of amplitude normalization, since it happens in a region where *Pg* maximum energy varies slowly with distance (Figure 3). The anomaly cannot be attributed to a change in the shallow structure either, because the *Pg* and *Lg* energy would also be affected. The best explanation is a structure-related effect with its origin at the crust-mantle boundary or in the uppermost part of the mantle. At such near offsets the *Pn* phase is not made of diving waves sampling a large thickness of the upper mantle, but is restricted to the head wave sampling the uppermost mantle. Possible explanations include lateral variations of the Moho dip and lateral changes in the *P* wave velocity or density at the top of the mantle.
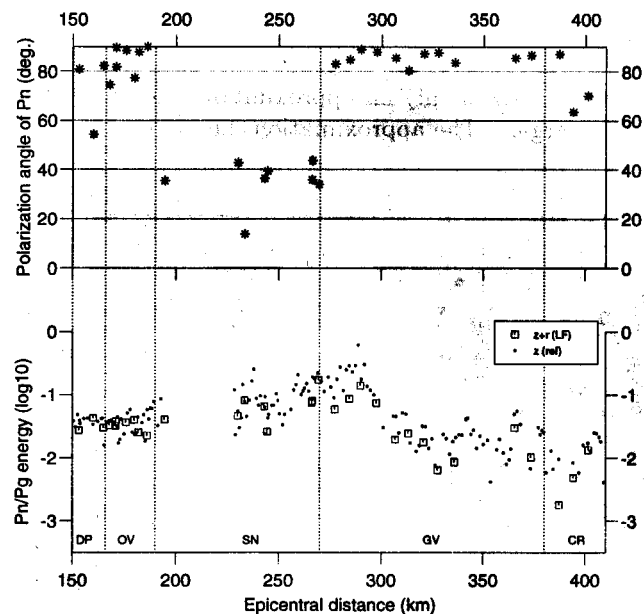
Figure 6. Variations with distance of the polarization angle of particle wave motion (top) and total energy (bottom) of the Pn phase, as measured from the seismograms normalized by the Pg maximum energy. The values of polarization angle and the energies plotted as open squares are measured from the radial and vertical components of the low-frequency data set. The dots in the bottom plot correspond to Pn energy values measured on the vertical seismograms of the refraction data set.

Numerical Simulations of *Sn* Wave Propagation

To find an explanation for the observed *Pn* amplitude anomaly, we compute *SH* synthetic seismograms in a 2-D medium including an irregular interface between two stratified media. The numerical method is the boundary integral equation method (BIEM) coupled with a discrete wavenumber representation of the source-radiated wave field [*Campillo*, 1987]. The 2-D approximation is justified, because the profile is almost perpendicular to the geological structures. The limitation to the *SH* case is sufficient, since *P-SV* coupling plays a negligible part in the variations of *Pn* amplitudes with offset. Synthetic seismograms are computed by using a 1-s Ricker wavelet as the source time function and for an explosive source at 10 km depth. This source depth is unrealistic, but it makes computations faster and has no influence on the results. As for *Pn* in real data, *Sn* energy is calculated by summing the squared amplitudes in a 4-s time window centered on the *Sn* arrival time. In the *SH* case the phase corresponding to *Pg*, defined as the wave train which propagates at a group velocity typical of crustal *P* waves (i.e., 5 to 6 km/s), is the *Lg* phase which propagates at a group velocity typical of crustal *S* waves (i.e., 3 to 3.5 km/s). Its energy is used to normalize the synthetic seismograms and compute the variations of the *Sn/Lg* energy ratio.

The first model tested is presented in Figure 7a. The crosses give the Moho depth measured by *Fliedner et al.* [1996], using travel time modeling of refraction and reflection data of the SSCD experiment. The small crustal root is modeled by a half period of a cosine function 180 km long (half wavelength) and 8 km thick (half peak-to-peak amplitude). With the simulation technique that we use, the difference in depth between the eastern and western ends cannot be accounted for without considering models with a much larger extent requiring longer computation times. Therefore all the models have the same Moho depth of 35 km under both eastern and western sides. The crust and upper mantle are considered at first as homogeneous with *S* wave velocities of 3.45 km/s and 4.60 km/s. With a Poisson's coefficient of 0.25 these values correspond to the average *P* wave velocities measured from the refraction work: 6.0 km/s and 8.0 km/s. Twenty-six receivers are located at the surface every 10 km between 160 and 410 km.

Synthetic seismograms computed for the model shown in Figure 7a are plotted in Figure 7b by using a reduction velocity of 4.6 km/s. Amplitudes are divided by the square root of the offset to simulate three-dimensional geometrical spreading from 2-D synthetic seismograms. The *Sn* wave appears as the first arrival with changes in apparent velocity due to the Moho topography. The large-amplitude arrival visible after 8 s at the first four receivers is the *Lg* phase. The direct wave is not computed to prevent contamination of the *Sn* phase. For purposes of clarity we plot only seismograms between
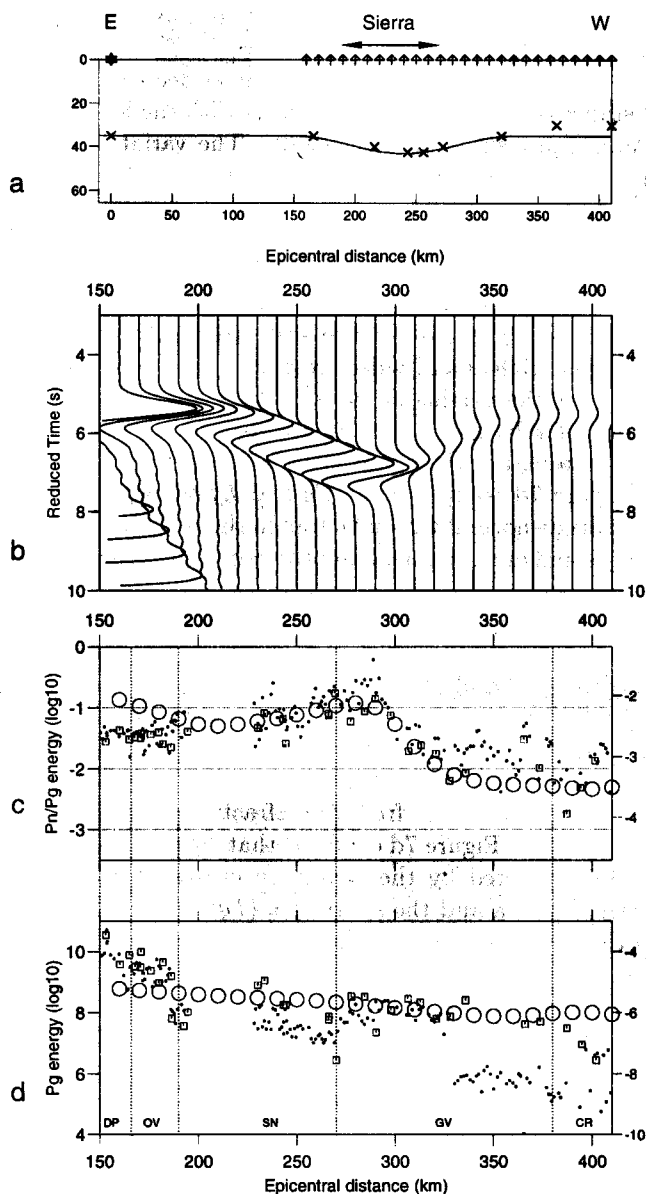
Figure 7. Results of the best fitting model. (a) Two-layer velocity structure used for computing synthetic seismograms. Note that the ratio of vertical to horizontal scale is 1.81. The markers on the surface show the location of the source (star at offset 0) and the 26 receivers. The Moho topography is computed to fit the depths inferred from SSCD reflection data (crosses, from *Fliedner et al.* [1996]). (b) Synthetic SH seismograms computed for the velocity model shown in Figure 7a. The reduction velocity is 4.60 km/s. Seismograms are plotted with offsets increasing from the right to the left. (c) Energy ratios Pn/Pg measured from the data (open squares and solid circles) and Sn/Lg computed from the synthetic seismograms of Figure 7b (large open circles) along the profile, as a function of the source-receiver offset. The left y axis corresponds to the real data, and the right y axis corresponds to values measured on the synthetic seismograms. (d) Variations with offset of the total energy of the Pg phase measured from the real data (open squares and solid circles) and of the Lg phase measured on the synthetic seismograms. As in Figure 7c, the left y axis corresponds to the real data, while the right y axis corresponds to the synthetics.

0 and 10 s, although 30-s seismograms have been computed.

Figure 7b shows that Sn amplitudes decrease from a distance of 290 km, which coincides with the location of the increase in apparent velocity. The variations with offset of the Sn/Lg total energy ratio computed from the synthetics are plotted as large open circles in Figure 7c. They are superimposed on the Pn/Pg energy ratio measured from the data and presented previously in Figure 6. Note that the real and synthetic data are plotted at the same vertical scale (represented on the left- and right-hand sides, respectively, of Figure 7c) but that the origins of the two axes are shifted. The range of relative Pn energy variations is the same in the data and in the synthetics.

Figure 7d compares the Pg and Lg energies used as amplitude normalization factors in the real data (closed circles and open squares) and the synthetic seismograms (large open circles). At offsets smaller than 200 km the shift between observations and synthetics is related to an underestimate of the Pg energy in the synthetics (Figure 7d) resulting from the lack of direct wave. At offsets larger than 200 km the synthetic data coincide with the observations, indicating that the observed Pn amplitude variations can be explained by the change in Moho depth deduced from the refraction work [*Fliedner et al.*, 1996]. Figure 7d confirms that Pg amplitudes are slightly affected by the change in crustal thickness in both the data and the synthetics (Lg). Therefore most of the Pn/Pg energy ratio anomaly of Figure 7c is a Pn amplitude anomaly.

Two mechanisms can explain the Pn energy increase. The most obvious one is the geometrical effect of the change in Moho dip. The upper halves of the two parts (descending and ascending) of the Moho topography act as defocusing lenses, whereas their bottom halves act as focusing lenses. Because of the propagation through the crust at the critical angle, the related amplitude anomalies appear at the surface with a shift of 26 km toward the west, which is precisely what we observe. The second mechanism is the diffraction of the incident Pn by the Moho topography, inducing the conversion of part of the wave train into crustal phases. The diffracted part would then be lost for further propagation as an interface wave. The Pn energy at large offsets would never gain back the energy level observed with a flat Moho, as it would if only focusing and defocusing effects are acting. We check that at 410 km the Pn energy is back at the same level as that for a flat Moho, an indication that the geometrical effect is dominant in the observed Pn amplification. The diffraction is weak because the Moho topography is smooth (maximum dip, 8°).

To investigate the sensitivity of the Sn/Lg energy ratio to the model parameters, we study the influence of the velocity contrast at the Moho and the Moho geometry. Figure 8a shows the results of the tests on the lower crustal velocity, keeping the same geometry as that in Figure 7a. To avoid shifting the anomaly to
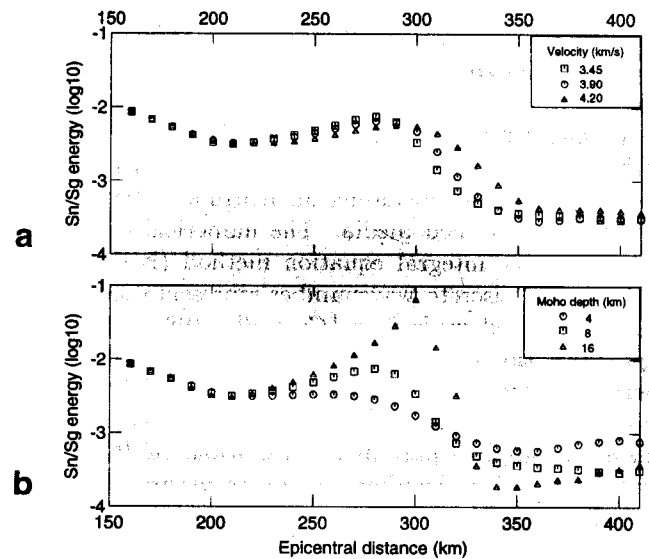
Figure 8. Influence of (a) the velocity contrast at the Moho and (b) the maximum Moho depth (below the average 35 km depth) on the computed Sn/Lg energy ratio. In both plots the reference model (plotted as squares) is the one presented in Figure 7.

larger offsets and to facilitate comparisons, we modify the S wave velocity only in the crustal root. The same velocity of 3.45 km/s is used in the upper 35-km-thick flat layer. Within the small root we test a high crustal velocity (3.90 km/s, corresponding to a 6.75-km/s P wave velocity) and a low upper mantle velocity (4.20 km/s, corresponding to 7.27 km/s in P). This second test is inspired by *Jones et al.* [1994] and *Savage et al.* [1994], who suggested that the Sierran crust is underlain by a low-velocity upper mantle, the "7.x layer". Figure 8a shows that the Sn amplitude anomaly is not sensitive enough to the velocity contrast to discriminate these models.

In a second test we verify the influence of the Moho geometry by changing its maximum depth (Figure 8b), keeping all the other parameters as in the first model. The amplitude increase of the Sn phase is very sensitive to the Moho dip. Neither the smaller (4 km) nor the larger (16 km) crustal root models match the observed energy variations of the Pn phase, as did the 8-km root of the first model. This is one more element in favor of the small crustal root inferred from the refraction work. Finally, combinations of the different parameters are used. Figure 9 shows that yet another model yields a correct fit to the general shape of the observed Pn amplitude variations with distance. It includes a crust of constant 35 km thickness and a cosine-shaped lens of 4.20 km/s anomalous upper mantle with the same horizontal wavelength as above (180 km) and the largest amplitude tested (16 km below Moho level). To fit the location of the Pn anomaly at the surface, the heterogeneity has to be shifted 40 km to the east with respect to the model of Figure 7a. Thus the deeper part of the
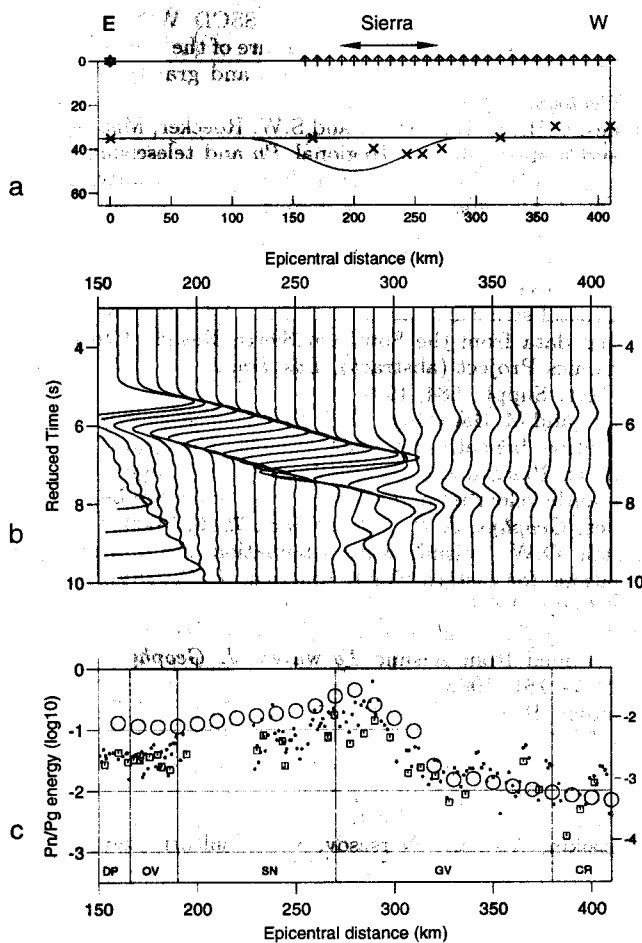
Figure 9. Results of the numerical simulations for a velocity structure including the 7.x layer of *Savage et al.* [1994]. (a) Velocity model. See Figure 7a for the meaning of the different markers. This model includes three different velocities: 3.45 km/s in the crust, 4.60 km/s in the mantle, and 4.20 km/s inside the upper mantle heterogeneity. (b) Synthetic seismograms (see Figure 7b caption). (c) Computed variations of the Sn/Lg energy ratio (large open circles) as compared to the observed variations (closed circles and open squares) (see Figure 7c caption).

low-velocity upper mantle is located under the high altitudes of the Eastern Sierra, and its structure is very similar to the one inferred by *Savage et al.* [1994] (Figure 9a). As a consequence the observed *Pn* amplitude anomaly is compatible with the two last models proposed for the deep structure of the Southern Sierra by the SSCD refraction team and by *Savage et al.* [1994].

A close comparison of Figures 7c and 9c shows that the first model with the Moho deflection gives a slightly better fit to the amplitude increase between 230 and 280 km and to the decrease between 290 and 360 km than the model with a lens of anomalous upper mantle. The stronger topography of the irregular interface in the second model induces a greater amplification of the head wave after 170 km, which is also clear on the seismograms of Figure 9b. Slight differences in the arrival

times of the *Sn* phase for the two models can be seen in Figures 7b and 9b. The main difference between the two models is the energetic secondary arrival of Figure 9b. This arrival can be interpreted as the interface wave traveling horizontally across the low-velocity anomaly at the crust-mantle boundary, unlike the earlier arrival, which propagates in the normal upper mantle beneath the heterogeneity. The late secondary arrival does not appear in the real data. Moreover, the second model with its thick lens of anomalous upper mantle does not fit the arrival times of the refracted and reflected waves [*Fliedner et al.*, 1996] or those of the teleseismic converted waves (R. Phinney and C. Jones, personal communication, 1995) recorded during the SSCD experiment.

Conclusions

The study of the variations of the crustal phase *Lg* and *Pg* total energies along our profile shows a regular decrease with distance except in the Great Valley basin, which amplifies both phases. Another influence of the geological structure on the *Pg* and *Lg* amplitudes is the change in polarization angle due to the thick sedimentary sequence of the Great Valley. It makes the *Lg* phase almost disappear on the vertical component, while the *Pg* phase is weaker on the horizontal components for stations in the valley. This observation demonstrates that interpretations of changes in amplitude of regional phases observed in sedimentary basins only from vertical component seismograms must consider changes in polarization angles.

Except for the amplification in the Great Valley, *Lg* and *Pg* amplitudes decrease with distance from the source, as predicted by the theoretical expressions of geometrical spreading and attenuation. No Q (Q_P and Q_S) anomaly is detected in the Sierra Nevada. We find that the *Pg* and *Lg* crustal phases propagate through the southern Sierra Nevada, suffering neither extinction nor attenuation related to the crustal structure or to the topography.

The main amplitude anomaly revealed by this study is a large and progressive increase of the *Pn* amplitude in the Sierra Nevada and the eastern quarter of the Great Valley, followed by an abrupt decrease 30 km west of the western limit of the exposed Sierran batholith. The change in *Pn* amplitude is located close to where its apparent velocity changes. The velocity change has been interpreted from refraction data to result from a localized change in Moho depth. Synthetic *SH* seismograms computed in simple crustal models show by analogy that the *Pn* amplitude increase observed in the Sierra Nevada and Eastern Great Valley is consistent with the presence of a small crustal root, as inferred from the SSCD refraction work [*Fliedner et al.*, 1996]. The variations in *Pn* amplitude are geometrical effects due to the Moho topography.

Numerical tests with different velocity models show that the Pn amplitude anomaly is not sensitive to the velocity constrast at the Moho, but it is strongly influenced by the Moho dip. A crustal thickening of 16 km does not match our observations, adding an argument in favor of the small crustal root. However, the "7.x layer" model of Savage et al. [1994] is also compatible with the observed anomaly, although the small Moho deflection gives a better fit to the details of the observed amplitude curve.

In general, this study confirms the unstable nature of the Pn amplitude, as compared to the much more stable Pg and Lg crustal phases. While the crustal waves have no amplitude variations across the Sierra Nevada, the Pn energy is amplified 10 times by minor Moho relief, amounting to 8 km over a distance of 180 km.

References

Baumgardt, D.R., Investigation of teleseismic Lg blockage and scattering using regional arrays, *Bull. Seismol. Soc. Am.*, 80, 2261-2281, 1990.

Campillo, M., Lg wave propagation in a laterally varying crust and the spatial distribution of the quality factor in Central France, *J. Geophys. Res.*, 92, 12604-12614, 1987.

Campillo, M., M. Bouchon, and B. Massinon, Theoretical study of the excitation, spectral characteristics and geometrical attenuation of regional seismic phases, *Bull. Seismol. Soc. Am.*, 74, 79-90, 1984.

Campillo, M., B. Feignier, M. Bouchon, and N. Béthoux, Attenuation of crustal waves across the Alpine range, *J. Geophys. Res.*, 98, 1987-1996, 1993.

Chavez, D.E., and K.F. Priestley, Measurement of frequency dependent Lg attenuation in the Great Basin, *Geophys. Res. Lett.*, 13, 551-554, 1986.

Chazalon, A., M. Campillo, R. Gibson, and E. Carreno, Crustal wave propagation anomaly across the Pyrenean Range, *Geophys. J. Int.*, 115, 829-838, 1993.

Chinn, D.S., B.L. Isacks, and M. Barazangi, High-frequency seismic wave propagation in western South America along the continental margin, in the Nazca plate and across the Altiplano, *Geophys. J. R. Astron. Soc.*, 60, 209-244, 1980.

Fliedner, M.M., S. Ruppert, and SSCD Working Group, Three-dimensional crustal structure of the Southern Sierra Nevada from seismic fan profiles and gravity modelling, *Geology*, 24, 367-370, 1996.

Jones, C.H., H. Kanamori, and S.W. Roecker, Missing roots and mantle "drips": Regional Pn and teleseismic arrival times in the Southern Sierra Nevada and vicinity, California, *J. Geophys. Res.*, 99, 4567-4601, 1994.

Kanasewich, E., Time sequence analysis in Geophysics, Univ. of Alberta Press, Edmonton, 1975.

Keller, R.G., S.D. Ruppert, A.D. Duran, and K.C. Miller, Crustal structure east of the Sierra Nevada based on seismic data from the Southern Sierra Nevada Crustal Dynamics Project (abstract), *Eos Trans. AGU, 75*(44), Fall Meet. Suppl., 584, 1994.

Ni, J., and M. Barazangi, High-frequency seismic wave propagation beneath the Indian Shield, Himalayan Arc, Tibetan Plateau and surrounding regions: High uppermost mantle velocities and efficient Sn propagation beneath Tibet, *Geophys. J. R. Astron. Soc.*, 72, 665-689, 1983.

Nuttli, O.W., Seismic wave attenuation and magnitude relations for eastern North America, *J. Geophys. Res.*, 78, 876-885, 1973.

Nuttli, O.W., Yield estimates of Nevada Test Site explosions obtained from seismic Lg waves, *J. Geophys. Res.*, 91, 2137-2151, 1986.

Phinney, R.A., C.H. Jones, and C.B. Parker, Reflection and refraction imaging of the crust under the Southern Sierra Nevada using local and regional earthquakes recorded by small arrays (abstract), *Eos Trans. AGU, 75*(44), Fall Meet. Suppl., 584, 1994.

Ruzaikin, A.I., I.L. Nersesov, V.I. Khalturin, and P. Molnar, Propagation of Lg and lateral variations of crustal structure in Asia, *J. Geophys. Res.*, 82, 307-316, 1977.

Savage, M.K., L. Li, J.P. Eaton, C.H. Jones, and J.N. Brune, Earthquake refraction profiles of the root of the Sierra Nevada, *Tectonics*, 13, 803-817, 1994.

Singh, S.K., and R.B. Herrmann, Regionalization of crustal coda Q in the continental United States, *J. Geophys. Res.*, 88, 527-538, 1983.

Wald, L.A., and T.H. Heaton, Lg and Rg waves on the California regional networks from the December 23, 1985 Nahanni earthquake, *J. Geophys. Res.*, 96, 12099-12125, 1991.

Walter, W.R., K.M. Mayeda, and H.J. Patton, Phase and spectral ratio discrimination between NTS earthquakes and explosions, I, Empirical observations, *Bull. Seismol. Soc. Am.*, 85, 1050-1067, 1995.

Wernicke, B., et al., Origin of high mountains in the continents: The Southern Sierra Nevada, *Science, 271*, 190-193, 1996.

D. Baumont, M. Campillo and A. Paul, Laboratoire de Géophysique Interne et Tectonophysique, Centre National de la Recherche Scientifique, and Université Joseph Fourier, BP 53X, 38041 Grenoble Cedex, France. (e-mail: apaul@lgit.observ-gr.fr)

D. Jongmans, Laboratoire de Géologie de l'Ingénieur et d'Hydrogéologie, Université de Liège, 4000 Liège, Belgium.

P. Malin, Department of Geology, Duke University, Durham, NC 27708.